

The role of gaps in digitized counterdiabatic QAOA for fully-connected spin models

Mara Vizzuso,^{1, a} Gianluca Passarelli,¹ Giovanni Cantele,² and Procolo Lucignano¹

¹*Dipartimento di Fisica “E. Pancini”, Università degli Studi di Napoli “Federico II”,
Complesso Universitario M. S. Angelo, via Cintia 21, 80126, Napoli, Italy*

²*CNR-SPIN, c/o Complesso Universitario M. S. Angelo, via Cintia 21, 80126, Napoli, Italy*

(Dated: November 13, 2024)

Recently, digitized-counterdiabatic (CD) corrections to the quantum approximate optimization algorithm (QAOA) have been proposed, yielding faster convergence within the desired accuracy than standard QAOA. In this manuscript, we apply this approach to a fully-connected spin model with random couplings. We show that the performances of the algorithm are related to the spectral properties of the instances analyzed. In particular, the larger the gap between the ground state and the first excited states, the better the convergence to the exact solution.

I. INTRODUCTION

In recent years, the field of quantum computing has experienced remarkable advancements, showing new ways for addressing computational challenges previously deemed impossible for classical computers. Among the others, Variational Quantum Algorithms (VQAs) have emerged as particularly versatile tools [1]. VQAs address optimization tasks by iteratively refining the parameters of a quantum circuit to minimize a desired cost function. This makes VQAs adaptable and versatile to different applications, spanning quantum chemistry simulations [2–4], machine learning [5, 6], and combinatorial optimization [7, 8].

An example of VQAs is the Quantum Approximate Optimization Algorithm (QAOA) [9]. QAOA serves as a variational technique tailored for tackling combinatorial optimization problems within gate-based quantum computing systems. In essence, combinatorial optimization consists in identifying, from a finite set of variables, the ones that minimize a desired cost function. This finds practical applications across various domains such as streamlining supply chain costs, optimizing vehicle routes, allocating tasks efficiently, and more [10–14]. In QAOA a combinatorial optimization problem is cast into the form of searching the approximate ground state of a spin Hamiltonian [15], achieved through a specific variational ansatz. This ansatz is expressed via a gate circuit depending on free parameters to be optimized using a classical computer minimization routine.

Many QAOA variants have proliferated over the years to further improve the performance of the original algorithm [16–36]. A non-exhaustive list includes: QAOA+[37], which improves the conventional QAOA adding an additional problem-independent layer with multiple parameters; adaptive-bias QAOA [26], introducing local fields to QAOA operators; adaptive QAOA [27], a QAOA variant iteratively selecting mixers based on a systematic gradient criterion; and recursive-QAOA [28], aiming to decrease problem size by eliminating unnecessary qubits through a non-local scheme. A promising variant is the digitized counterdiabatic QAOA (QAOA-CD) [33–35], which incorporates an additional driving Hamil-

tonian inspired by quantum shortcuts to adiabaticity [38–40]. This additional Hamiltonian leads to faster convergence to the ground state energy, allowing for a reduction in the circuit depth.

In this paper, we apply the variant of QAOA originally developed in Ref. [40] to study the randomly weighted MaxCut problem on 2-regular graphs, to explore its suitability to fully-connected graphs in which long-range all to all interactions significantly amplify the computational complexity with respect to local interactions. In this setting, our goal is twofold. On the one hand, we will show that the counterdiabatic variants of QAOA are also feasible for fully-connected models. On the other hand, we will show through an in-depth statistical study that the performance of QAOA and its variants depend on the spectral properties of the target Hamiltonian. We can in fact distinguish “easy” and “hard” Hamiltonians depending on the value of the gap between the target ground state and the first excited states, in a similar fashion to adiabatic quantum computing (AQC). In AQC, the minimum *instantaneous* gap between the time-dependent ground state and first excited state classifies the hardness of the optimization problem as it determines the minimum time scale necessary for successful adiabatic state preparation [41]. In QAOA, instead, where continuous evolutions are replaced by digital steps and it is not possible to identify a continuous time-dependent generator of the quantum circuit, this role is played by the gap of the *target* Hamiltonian. This is a consequence of the fact that the variational procedure is more complicated for problem Hamiltonians with small gaps, as we are going to discuss later on.

The paper is organized as follows. We introduce our model Hamiltonian in Sec. II and review QAOA and its counterdiabatic corrections in Sec. III. In Sec. IV, we present the outcomes of our numerical analysis. Finally, we summarize our findings in Sec. V.

II. MAXCUT MODEL

Combinatorial optimization problems are relevant to economics and finance [42], they include the Traveling Salesman Problem (TSP) [43], the Minimum Spanning Tree Problem (MST) [44], the Knapsack Problem [45], the MaxCut prob-

^a mara.vizzuso@unina.it

lem [46], and many others [47–49]. In particular we here focus on quadratic unconstrained binary optimization (QUBO) that can be formally defined as follows: given a discrete set K made of N binary variables and a function $f(\vec{x})$ that maps each item \vec{x} from K to a continuous set, the objective is to find the optimal combination of elements, denoted by \vec{x}^* , that minimizes the function $f(\vec{x})$.

Given a graph $G(E, V)$, defined as a collection of vertices (V set) interconnected by edges (E set) the concept of a Maximum Cut arises, denoting a partition that cuts off the greatest number of edges between two separate sets of vertices. This partition, termed a *cut*, is characterized by a size representing the count of cut edges, which must surpass the size of any alternative partition to qualify as the Maximum Cut. The pursuit of this Maximum Cut constitutes a computational challenge categorized under NP-hard problems [50] and is recognized as the MaxCut problem. Classically we define the cost function $f(\vec{x})$ whose maximum is the solution of the MaxCut problem on a graph $G(E, V)$ as:

$$f(\vec{x}) = \frac{1}{2} \sum_{i,j \in G(E,V)} (1 - x_i x_j). \quad (1)$$

We suppose that the graph $G(E, V)$ has N vertices. On each vertex i the variable x_i can assume either the value $x_i = +1$ or $x_i = -1$. The set of all possible states, in the form (x_1, x_2, \dots, x_N) has dimension 2^N . The MaxCut consists in partitioning the graph into two subgraphs A and B such that all the elements in A assume the value $x_i = +1$, and all the elements in B take the value $x_i = -1$ cutting the maximum number of edges.

Finding the maximum of a cost function f over a set of binary variables \vec{x} is the same as calculating the ground state energy of a classical spin Hamiltonian. Classical spins can be set at the vertices of a graph whose edges depend on the Hamiltonian connectivity. Therefore solving a QUBO is the same as finding the ground state of an Ising problem [15]. Various methodologies derived from statistical and quantum physics can be employed to address this challenge, including techniques such as Quantum and Simulated Annealing (QA and SA respectively) [41, 51–61], along with the QAOA.

II.1. Fully-connected spin model

We associate a Pauli operator σ_i^Z to each site i of the graph. The (dimensionless) Hamiltonian describing the MaxCut for a random fully-connected spin model is

$$H_T = \sum_{i < j}^N J_{ij} \sigma_i^Z \sigma_j^Z, \quad (2)$$

where σ_i^Z, σ_j^Z are the Pauli matrices acting on respectively the i^{th} and j^{th} spins and $J_{ij} = \mathcal{U}([-1, 1])$ are random couplings distributed according to the uniform distribution \mathcal{U} in the given range. The cost function of QAOA, as discussed in Sec. III, is given by the expectation value of H_T on a parametric quantum circuit. As a proof of principle we focus on

random instances with a small number of qubits, $N = 5$ (in Appendix A, we show that our results also hold for larger systems), and analyze $n = 600$ samples (which gives an accurate sampling of the coupling distribution without requiring unfeasible computational resources) of the disordered interactions, each of them with different couplings J_{ij} . In the case $J_{ij} = 1$ finding the ground state of the Hamiltonian of Eq. (2) is the same as finding the maximum of the cost function f defined in Eq. (1). Due to the Z_2 symmetry of the Hamiltonian of Eq. (2) all the eigenvalues are doubly degenerate.

III. QAOA AND VARIANTS

QAOA is a hybrid quantum-classical algorithm proposed by Farhi et al [9]. It consists of a quantum part and a classical part. The objective of the algorithm is to find the ground state of a target Hamiltonian H_T . The algorithm works as follows. We consider two Hamiltonians: H_T , representing our target Hamiltonian whose ground state solves our optimization problem, and H_X , a one-body Hamiltonian easy to diagonalize, encoding quantum fluctuations:

$$H_X = \sum_{i=1}^N \sigma_i^X, \quad (3)$$

where σ_i^X is a Pauli matrix associated with site i . The ground state of Eq. (3) is

$$|0\rangle = \frac{1}{\sqrt{2^N}} \bigotimes_{i=1}^N (|\uparrow\rangle_i - |\downarrow\rangle_i), \quad (4)$$

where $|\uparrow\rangle_i$ and $|\downarrow\rangle_i$ are eigenstates of the σ_i^Z operator associated with the i^{th} site.

The algorithm consists in transforming $|0\rangle$ using a set of unitaries depending on H_X and H_T and on variational coefficients that must be optimized classically in order to minimize the expectation value of the target Hamiltonian on the trial state.

The trial wavefunction is chosen as

$$|\psi^{(p)}(\vec{\beta}, \vec{\gamma})\rangle = \left(\prod_{k=1}^p U(\beta_k, H_X) U(\gamma_k, H_T) \right) |0\rangle \quad (5)$$

where

$$U(\theta, H) = e^{-i\theta H}. \quad (6)$$

The wavefunction $|\psi^{(p)}\rangle$ depends on the $2p$ parameters $\vec{\beta} = (\beta_1, \dots, \beta_p)$ and $\vec{\gamma} = (\gamma_1, \dots, \gamma_p)$, where p represents the number of QAOA steps. The cost function to minimize is

$$E^{(p)}(\vec{\beta}, \vec{\gamma}) = \langle \psi^{(p)}(\vec{\beta}, \vec{\gamma}) | H_T | \psi^{(p)}(\vec{\beta}, \vec{\gamma}) \rangle. \quad (7)$$

QAOA consists in finding *classically* (i.e., on a classical computer) $\vec{\beta}^*$ and $\vec{\gamma}^*$ that minimize the function in Eq. (7). $|\psi^{(p)}(\vec{\beta}^*, \vec{\gamma}^*)\rangle$ represents an approximation of the true ground

state of H_T [Eq. (2)] after p steps. Increasing the number $2p$ of variational parameters improves the “expressivity” of the trial wave function allowing for better and better approximations of the state we are looking for. In some cases [62], QAOA allows us to get the exact solution in a finite number of steps p . However, in most cases, there is only an asymptotic convergence to the exact ground state of H_T by increasing the number of steps.

Next, we describe digitized-counterdiabatic variants of QAOA, which allow improving the accuracy of QAOA at any circuit depth p [40]. This algorithm is inspired by the counterdiabatic potentials [63], included in the QAOA algorithm via next-order terms of the Baker-Hausdorff-Campbell (BHC) expansion [64]. One gets the so-called QAOA-CD [33, 35] by stopping at the first-order correction. At each step p of QAOA-CD, the QAOA state is not only transformed by the unitaries $U(\beta, H_X)$ and $U(\gamma, H_T)$ as in Eq. (5), but also by an additional operator U_{CD} , as follows:

$$|\psi_{CD}^{(p)}(\vec{\beta}, \vec{\gamma}, \vec{\alpha})\rangle = \left(\prod_{k=1}^p U(\beta_k, H_X) U(\gamma_k, H_T) U_{CD}(\alpha_k) \right) |0\rangle, \quad (8)$$

where we see another p -dimensional vector of parameters $\vec{\alpha} = (\alpha_1, \dots, \alpha_p)$ and

$$U_{CD}(\alpha) = e^{-\alpha[H_X, H_T]}. \quad (9)$$

Looking at Eq. (7), we can easily generalize a new cost function $E_{CD}^{(p)}(\vec{\beta}, \vec{\gamma}, \vec{\alpha})$ that counts $3p$ parameters per step.

In QAOA-2CD, this process can be further improved adding the next term in the BHC expansion [40]. Therefore the trial wave function becomes

$$|\psi_{2CD}^{(p)}(\vec{\beta}, \vec{\gamma}, \vec{\alpha}, \vec{\delta}, \vec{\zeta})\rangle = \left(\prod_{k=1}^p U(\beta_k, H_X) U(\gamma_k, H_T) U_{CD}(\alpha_k) U_{2CD}(\delta_k, \zeta_k) \right) |0\rangle, \quad (10)$$

where $\vec{\delta} = (\delta_1, \dots, \delta_p)$ and $\vec{\zeta} = (\zeta_1, \dots, \zeta_p)$ are p -dimensional vectors, and

$$U_{2CD}(\delta, \zeta) = e^{i\delta[H_X, [H_X, H_T]] - i\zeta[H_T, [H_X, H_T]]}, \quad (11)$$

and the new cost function is $E_{2CD}(\vec{\beta}, \vec{\gamma}, \vec{\alpha}, \vec{\delta}, \vec{\zeta})$, depending on $5p$ parameters. The variants QAOA-CD and QAOA-2CD differ from QAOA only in the construction of the quantum part of the algorithm, the classical minimization changes only for the number of parameters of the cost function at any given step.

In order to analyze the accuracy of these algorithms, we introduce the *residual energy* and the *fidelity* at each step p . The residual energy is defined as:

$$\varepsilon_{\text{res}}^{(p)}(\vec{\beta}, \vec{\gamma}) = \frac{E_p(\vec{\gamma}, \vec{\beta}) - E_{\min}}{E_{\max} - E_{\min}}, \quad (12)$$

where $E_{\min(\max)}$ is the minimum (maximum) eigenvalue of the Hamiltonian of Eq. (2). This is trivially generalized to QAOA-CD [$\varepsilon_{CD}^{(p)}(\vec{\beta}, \vec{\gamma}, \vec{\alpha})$] and QAOA-2CD [$\varepsilon_{2CD}^{(p)}(\vec{\beta}, \vec{\gamma}, \vec{\alpha}, \vec{\delta}, \vec{\zeta})$].

We can further introduce the fidelity, which for QAOA is

$$F^{(p)}(\vec{\beta}, \vec{\gamma}) = \left| \langle \psi_T | \psi^{(p)}(\vec{\gamma}, \vec{\beta}) \rangle \right|^2, \quad (13)$$

where $|\psi_T\rangle$ is the ground state of H_T [see Eq. (2)]. We can easily generalize this equation to QAOA-CD [$F_{CD}^{(p)}(\vec{\beta}, \vec{\gamma}, \vec{\alpha})$] and QAOA-2CD [$F_{2CD}^{(p)}(\vec{\beta}, \vec{\gamma}, \vec{\alpha}, \vec{\delta}, \vec{\zeta})$].

IV. RESULTS

In this section, we discuss results achieved by studying the disordered fully-connected spin model of Eq. (2) within the QAOA, QAOA-CD, and QAOA-2CD frameworks. The classical optimization is performed using the L-BFGS-B method [65]. For each algorithm (QAOA, QAOA-CD, QAOA-2CD) and at each step, we start the optimization with 20 randomly selected sets of initial angles, and select the best result from these optimizations. While this approach does not guarantee a global optimum, the optimization can be refined by increasing the number of initial angle choices when needed. Our results are averaged over a set of $n = 600$ random instances. Disorder-averaged quantities are calculated as

$$\langle K \rangle = \frac{1}{n} \sum_{i=1}^n K_i \quad (14)$$

$$\sigma_K = \sqrt{\frac{1}{n} \sum_{i=1}^n (K_i - \langle K \rangle)^2}, \quad (15)$$

where K_i is a generic observable as evaluated on a single instance characterized by a set of couplings $J_{jk}^{(i)}$ and $\langle K \rangle$ and σ_K are respectively the mean value and standard deviation of K .

The ground state of Eq. (2) has a double degeneracy, therefore the fidelity of Eq. (13) is computed as

$$F^{(p)} = |\langle \psi_T^1 | \psi^{(p)}(\vec{\gamma}^*, \vec{\beta}^*) \rangle|^2 + |\langle \psi_T^2 | \psi^{(p)}(\vec{\gamma}^*, \vec{\beta}^*) \rangle|^2, \quad (16)$$

where ψ_T^1 and ψ_T^2 are the two degenerate eigenstates corresponding to the ground-state energy E_{\min} of the Hamiltonian of Eq. (2).

The fidelity of Eq. (16) as well as the residual energy of Eq. (12) are used in the following to assess the performances of the algorithm and eventually connect them with the spectral properties of H_T . In quantum annealing [41, 54, 66], the minimal gap during the annealing dynamics determines the fidelity of the algorithm due to the occurrence of Landau-Zener transitions. In QAOA such strict relation between the gaps and the fidelity is not known nor well established, however a dense spectrum in the vicinity of the ground state, makes the system more prone to be “captured” by local minima during the hybrid optimization procedure [67]. To highlight the role of the gaps in the QAOA, in the following we will relate the QAOA performances for various instances keeping track of the distance between ground and the first excited state. In this paper we define this quantity as Δ_{eg} .

First of all, in Fig. 1(a), we show Δ_{eg} for all the $n = 600$ instances, which will be used as a reference in the following. We see that the majority of random instances have small gaps, but the tail of the distribution extends up to $\Delta_{eg} \sim 5$.

Then in Figs. 1(b,c) we show the residual energy and the fidelity as a function of p (the number of steps) for the three considered algorithms: QAOA, QAOA-CD and QAOA-2CD. The full lines represent the averages over the random instances, while the shadowed areas represent the respective standard deviations. As expected, we see that in all algorithms the trial state gets closer and closer to the target ground state as the circuit depth is increased, as shown by both the residual energy decreasing towards zero and the fidelity going up to one. Overall, QAOA-2CD gives the best results not only in terms of average value but also in terms of statistical standard deviation, both for the residual energy ε_{res} and for the fidelity F .

In the insets of Figs. 1(b,c) we also plot the standard deviations. By increasing the circuit depth, the standard deviations always decrease, except for a nonmonotonic behavior of the standard deviation of the fidelity for QAOA and QAOA-CD at low p . After $p^* = 6$ both the residual energy and the fidelity of the QAOA-2CD reach their limiting values, with negligible standard deviation, which means that we have reached the exact solution for almost all the instances.

IV.1. QAOA

In Fig. 2(a) we show the residual energy as a function of the number p of iterations of QAOA. Each grey line corresponds to the residual energy $\varepsilon_{\text{res},i}^{(p)}$ for a random instance, while the red bold curve indicates the average residual energy $\langle \varepsilon_{\text{res}} \rangle$ over all the n instances. The average residual energy at the step $p = 10$ is of the order of $\langle \varepsilon_{\text{res}}^{(10)} \rangle \simeq (2 \pm 3) \cdot 10^{-3}$, consistent with a zero residual energy at large p which means that, on average, QAOA gives a good approximation of the exact solution at $p = 10$. However the finite standard deviation indicates that some of the instances have yet to converge to their respective ground states, justifying the need for counterdiabatic corrections at finite p .

Is it possible to identify a common pattern among the instances that converge more slowly? In order to answer this question, we investigate the connection between the gap Δ_{eg} and complexity of the algorithm, following what is done in Ref. [68] for quantum annealing. In Figs. 2(b–d), we show scatter plots of the residual energy of each instance as a function of its gap Δ_{eg} , at some fixed steps p . In particular, we split the sorted gaps into three sets of equal cardinality (200 instances per set): in **I** there are problems with $\Delta_{eg} \in [0, 0.44]$, in **II** problems with $\Delta_{eg} \in [0.44, 1.02]$ and in **III** problems with $\Delta_{eg} \in [1.02, 4.74]$. In panel (b) we show the scatter plots for $p = 1$, in (c) those for $p = 2$ and in (d) those for $p = 7$. In panel (b), with $p = 1$, we see that the larger is the gap the bigger is the residual energy; this behavior is confirmed by the average value of residual energy in each region. The reason is that, at the first steps of QAOA, the parameters are not sufficient to accurately describe the problem’s ground state. As

a result, higher energy components of the QAOA variational guess over the computational basis states are detrimental for the algorithm. Starting from step $p = 2$ we note that this trend reverses and becomes more and more marked as the number of steps p increases, as we see comparing panels (c) and (d). In panel (c) the average residual energies of the regions **II** and **III** have similar values, then in the panel (d), for $p = 7$, the average in the region **III** is lower than that in region **I**. The numerical values of the average residual energies in each region can be found in Appendix A.

The connection between Δ_{eg} and the performance of the algorithm becomes more evident if we look at the fidelity, shown in Fig. 3. In Fig. 3(a) we show the fidelity of QAOA as a function of the step p , and in Figs. 3(b–d) we show scatter plots of the fidelity as a function of the gap Δ_{eg} at fixed step. In panel (a) we see that the average fidelity at $p = 10$ is close to one, but there is a large standard deviation σ_F . This behavior differs from ε_{res} , for which QAOA at step $p = 10$ provides a value much closer to its limit value and a much smaller standard deviation.

As we mentioned above, the residual energy measures the distance of the QAOA cost function from the true ground state energy, while the fidelity returns the overlap between the trial state at the end of the optimization procedure and the exact ground state. We can expect that the performance of the algorithm in terms of residual energy will appear to be generally better than that in terms of the fidelity both in terms of averages and standard deviations at any fixed step. Indeed, the algorithm is conceived to give the best answer for the residual energy, whereas the fidelity is computed after the optimal values $\vec{\beta}^*$ and $\vec{\gamma}^*$ at the given step p are obtained. Our results confirm such a picture, as shown in Appendix A. A similar picture is also valid for the other analyzed QAOA variants. On the other hand, comparing the results of Figs. 2 and 3 we can notice that in the case of the fidelity, unlike the residual energy, starting from $p = 1$ the instances corresponding to larger Δ_{eg} yield a better fidelity, showing an increasing trend with respect to the value of Δ_{eg} .

In the context of Quantum Annealing (QA), the relationship between the minimum gap along the dynamics and the complexity of the algorithm is well established. This is due to the adiabatic theorem, as outlined for instance, in Refs. [41, 69], which indicates that, during dynamics, the probability of having Landau-Zener transitions increases when the gap becomes smaller. However, this result is unexpected for QAOA, where we are not making a real time dynamics, but we only care about the “final time” results. Moreover, QAOA and QA are strictly related only in the $p \rightarrow \infty$ limit, which is not the case here. Therefore, in principle, we cannot fully explain the relationship between Δ_{eg} and the complexity of the algorithm in terms of the connection between QA and QAOA.

However, the correlation between Δ_{eg} and the values of residual energy and fidelity in QAOA could be related to the fact that in the presence of a dense spectrum of the Hamiltonian H_T there is a large likelihood of identifying local minima in close proximity to the ground state energy. To better understand why small gaps influence the performance of QAOA, we analyzed the path followed by our optimizer routine for

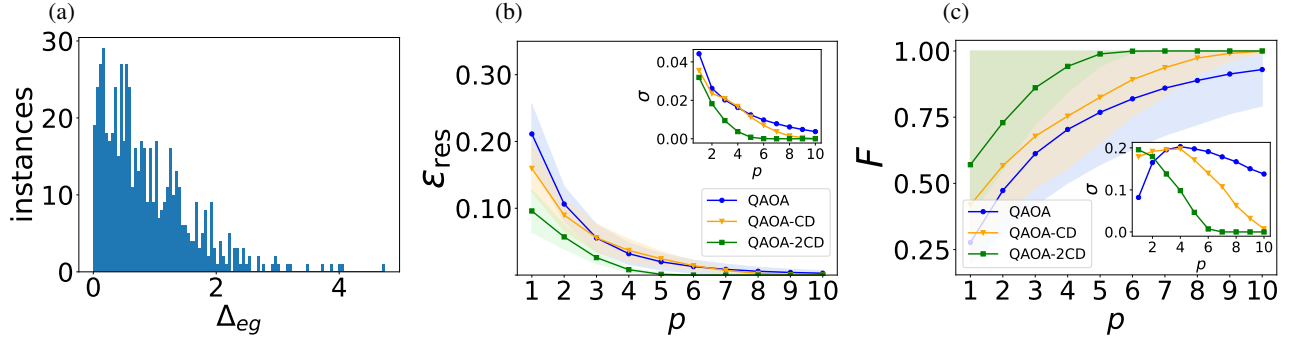


FIG. 1. (a) Distribution of the gap between the ground state and the first excited state (Δ_{eg}) among the $n = 600$ instances. (b) Residual energy and (c) fidelity in QAOA (blue curves), QAOA-CD (orange curves) and QAOA-2CD (green curves), as a function of the algorithms' step. The insets show the standard deviation for all the algorithms at each step p . At fixed step p , QAOA-2CD provides smaller residual energy and larger fidelity than the other methods.

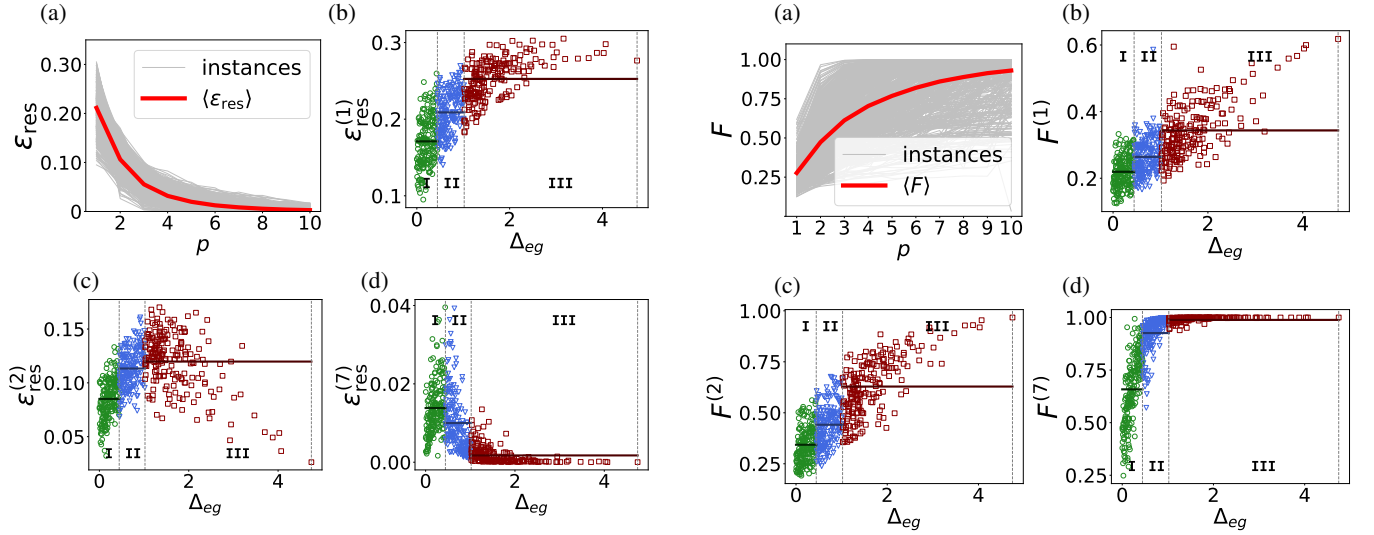


FIG. 2. (a) Residual energy versus QAOA step p . Grey lines represent $\varepsilon_{res,i}^{(p)}$ of all the $n = 600$ random instances and the red line their average value $\langle \varepsilon_{res} \rangle$. (b-d) Residual energy $\varepsilon_{res,i}^{(p)}$ as a function of the minimal gap Δ_{eg} for QAOA at steps (b) $p = 1$, (c) $p = 2$ and (d) $p = 7$. Three distinct regions based on the energy gap separating the ground state from the first excited state can be singled out for each instance: **I**-zone (green circles), corresponding to instances with $\Delta_{eg} \in [0, 0.44]$, **II**-zone (blue triangles) for instances with $\Delta_{eg} \in [0.44, 1.02]$, **III**-zone (red squares) for instances with $\Delta_{eg} \in [1.02, 4.74]$. The horizontal line within each sector depicts the corresponding average value of that sector. We see that for $p = 1$ these average values grow with increasing of Δ_{eg} . This trend starts to change from step $p = 2$ (panel c), whereas **III**-zone (panel d) shows a trend inversion (average value decreasing with the minimal gap).

three instances characterized by different values of the spectral gap, one per each zone, at the first step of QAOA, where the parameter space is two-dimensional and can be visualized. Our analysis shows that in all three cases the minimizer can quickly find the global minimum regardless of the gap, but the variational ansatz itself is a worse approximation of the true ground state when the minimum gap is smaller. In order to

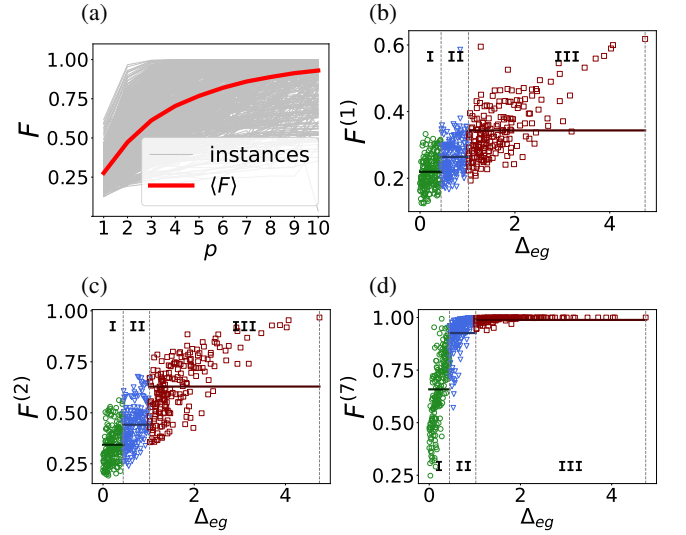


FIG. 3. (a) Fidelity versus QAOA step p . Grey lines represent values $F_i^{(p)}$ of all $n = 600$ random instances and the red line their average value $\langle F \rangle$. (b-d) Fidelity $F_i^{(p)}$ as a function of the minimal gap Δ_{eg} for QAOA at step (b) $p = 1$, (c) $p = 2$ and (d) $p = 7$. In panels (b-d) the three distinct regions described in caption of Fig. 2 are evidenced. The horizontal line within each sector depicts the corresponding average value of that sector. For each step p the fidelity closest to one is obtained for instances with Δ_{eg} belonging to **III**-zone.

better understand how the gap is important in the minimizer, the end of section IV.2 focuses on different roles played by the residual energy and the fidelity in finding the solution for QAOA and QAOA-2CD.

IV.2. QAOA-CD and QAOA-2CD

In this section, we will investigate whether QAOA-CD and QAOA-2CD confirm the dependence on the H_T minimum gap found in QAOA. Furthermore, these algorithms will be com-

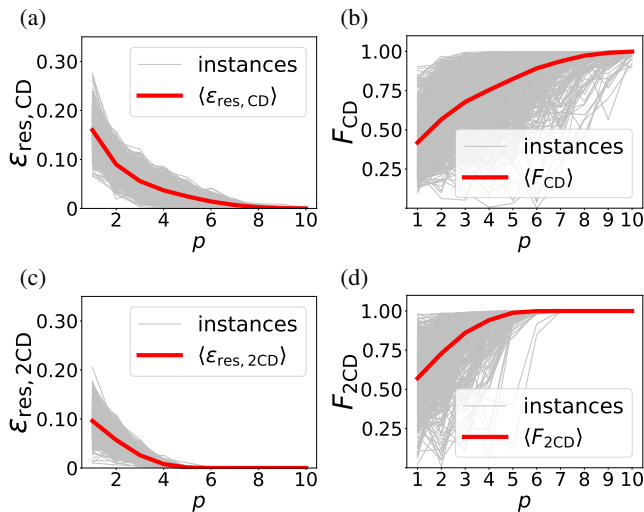


FIG. 4. (a) Residual energy and (b) fidelity of QAOA-CD versus step p . (c) Residual energy and (d) fidelity of QAOA-2CD versus p . The grey lines represent values of all the instances and the red line represents their respective averages.

pared to find out which one of them yields the optimal results in terms of average value and standard deviation for the residual energy and the fidelity. In order to make a fair comparison, we apply QAOA-CD and QAOA-2CD to the same instances of the fully-connected spin model analyzed for QAOA.

In Fig. 4, we present the residual energies and fidelities as a function of p for both QAOA-CD and QAOA-2CD. The grey lines represent the single instances, while the red ones represent the average values. Fig. 4(a,b) shows the performance of QAOA-CD. We observe that there is a step $p = 8$ in the residual energy plot after which the standard deviation is negligible. This feature has not been observed in standard QAOA, see Fig. 2. The QAOA-CD fidelity at $p = 10$ has a smaller standard deviation than the QAOA one and converges to a value very close to one.

In Fig. 4(c,d) we present the residual energy and the fidelity for QAOA-2CD. Similarly to QAOA-CD, there is also a step p for the residual energy in QAOA-2CD beyond which the standard deviation becomes close to zero. In this case, specifically, this happens at $p = 5$, earlier than for QAOA-CD.

Concerning the fidelity, in contrast to QAOA and QAOA-CD, where the standard deviation always remains nonzero up to $p = 10$, the fidelity in QAOA-2CD has a negligible error beyond the $p = 6$ step. In particular, before convergence, at the $p = 6$ step it is about ten times smaller than that found at the same step in QAOA and QAOA-CD.

Instances with $\Delta_{eg} \sim 0$ exhibit quasi-degeneracy between the ground and first excited states, leading to the QAOA state converging to a solution that reflects an overlap between these states [see Fig. 3(a)]. This behavior contrasts with the QAOA-2CD state, where, by step $p = 7$, the fidelity reaches 1 [see Fig. 4(d)]. From this observation, it appears that the role of the counterdiabatic correction in QAOA is analogous to that of the counterdiabatic potential in quantum annealing: both prevent transitions from the ground state to excited states, regardless

of the system's gap Δ_{eg} . The key distinction is that in QA, gaps are dynamical, while in QAOA, Δ_{eg} pertains to the gap of the target Hamiltonian H_T .

The residual energy decreases by increasing the order of the BHC expansion, following the opposite behavior as the fidelity. However, before convergence, its standard deviation is smaller than the one of the fidelity, as shown explicitly in Appendix A, where we report the numerical values of the average fidelities and residual energies in the three algorithms. Here in the main text we instead summarize these results visually in Fig. 5, where we plot the fidelity, the residual energy and their respective standard deviations in the form of heatmaps, for all analyzed algorithms and steps p . We generally see that QAOA-2CD is the algorithm yielding the best performances in terms of both metrics. For instance, the darker area in the top left panel, representing fidelities close to one, and the lighter area in the top right panel, showing small values of the residual energy, both occur at large steps p in correspondence of the QAOA-2CD line, where, correspondingly, their respective standard deviations vanish.

Finally, we study the performance of QAOA-2CD in each of the three separate zones identified by the ranges of the final gaps Δ_{eg} , in terms of residual energy and fidelity. We report our results in Fig. 6, where we study these quantities for two fixed steps of the algorithm: $p = 1$, panels (a,c), and $p = 2$, panels (b,d).

Concerning the fidelity in Figs. 6(a,b), we confirm the same trend seen in QAOA: the larger the gap, the closer the fidelity is to one. The solutions found in region **III** are closer to the real target state than the solutions found in region **I** for both steps p displayed. In fact, for steps $p = 1, 2$, the average values show a growth trend that brings the average fidelity very close to the solution in region **III**.

Regarding the residual energy, see Figs. 6(c,d), we observe a non monotonic dependence of the average residual energy as a function of Δ_{eg} , shown by the fact that, in region **II**, the average residual energy is higher than in region **I**. This pattern is found both for $p = 1$ and $p = 2$. This is in contrast with the QAOA results, shown in Fig. 2, which only display the same pattern starting from later steps (for instance, $p = 2$).

These observations are also valid for all other steps before convergence, as detailed in Appendix A, where we report the numerical values obtained by our analysis for other steps p , for the fidelity and the residual energy, in the three zones. At fixed p , the average value of the fidelity of QAOA-2CD in each region is generally closer to one than the average fidelity of QAOA. Besides, the standard deviation of the fidelity for all algorithms is smaller for problems characterized by a larger final gap, and also convergence requires fewer steps.

In Fig. 7 we examine three instances from distinct zones. In particular we focus on the instance with $\Delta_{eg} = 0.0021$ from **I**-zone (green curve), which has the smallest Δ_{eg} among all the instances analyzed; instance with $\Delta_{eg} = 1.9845$ from **II**-zone (blue curve); and instance with $\Delta_{eg} = 4.7457$ from **III**-zone (orange curve), the instance with the largest value of Δ_{eg} . In particular Fig. 7(a, b) shows the fidelity of these three instances with the ground state of H_T , $|\psi_T\rangle$ for QAOA and QAOA-2CD respectively. In Fig. 7(c, d) we represent the

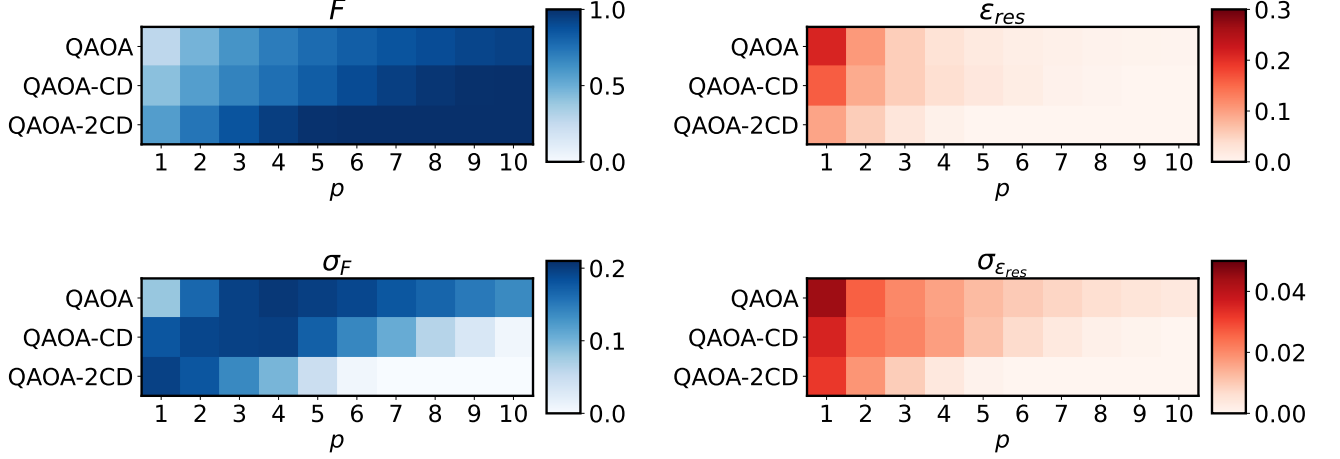


FIG. 5. Fidelity F (top left), its standard deviation σ_F (bottom left), residual energy ε_{res} (top right) and its standard deviation $\sigma_{\varepsilon_{\text{res}}}$ (bottom right) as a function of the step p , as calculated with all three methods (QAOA, QAOA-CD, QAOA-2CD) after averaging over the $n = 600$ random instances. We clearly see the residual energy decreasing towards zero and the fidelity increasing towards one as the step increases. The best performances are obtained with QAOA-2CD.

overlap between QAOA and QAOA-2CD respectively and the first excited state.

By comparing panels (a) and (c), we observe that, at convergence, the instance with the smallest gap (orange curve) in QAOA exhibits an overlap between the ground and first excited states. This is because, with a very small Δ_{eg} , the ground and

first excited states are quasi-degenerate, so QAOA effectively finds the solution in the subspace spanned by both states. However, in panels (b) and (d), we see that counterdiabaticity can resolve this quasi-degeneracy: despite requiring more steps p than other instances, the instance with the smallest gap in QAOA-2CD converges to the true ground state, despite the degeneracy.

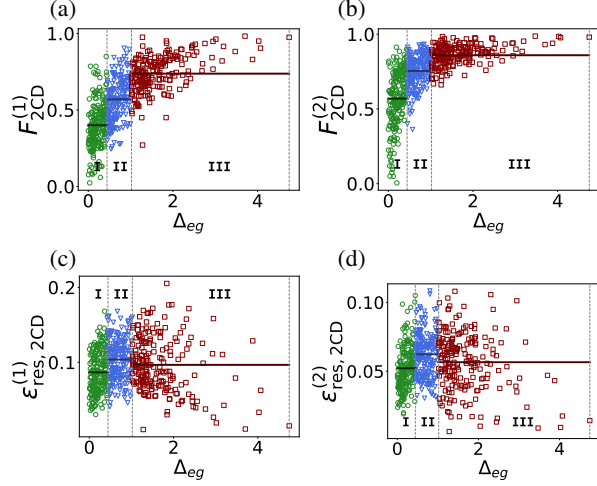


FIG. 6. Fidelity $F_i^{(p)}$ of QAOA-2CD for all $n = 600$ random instances versus Δ_{eg} for $p = 1$ (a) and $p = 2$ (b). Each point in the scatter plot represents the fidelity $F_{2\text{CD},i}^{(p)}$ for a single instance. Residual energy $\varepsilon_{2\text{CD},i}^{(p)}$ for all $n = 600$ different instances vs Δ_{eg} of QAOA-2CD for $p = 1$ (c) and $p = 2$ (d). Graphs delineate three distinct regions based on the energy gap Δ_{eg} , as illustrated in caption of Fig. 2. The horizontal line within each sector depicts the corresponding average value of that sector. Fidelity in QAOA-2CD increases with Δ_{eg} as for QAOA. It is not possible to appreciate a specific behavior for residual energy.

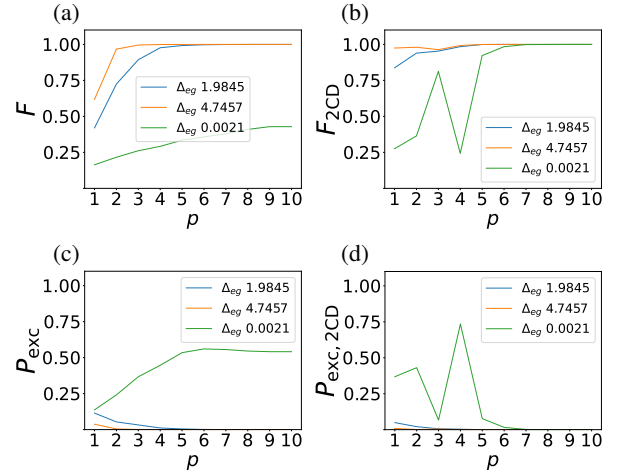


FIG. 7. (a) Fidelity between the QAOA state and the true ground state. (b) Excited-state probability of the optimal QAOA state. (c) Fidelity between the QAOA-2CD state and the true ground state. (d) Excited-state probability of the optimal QAOA-2CD state. Results are shown for three instances with different gap values Δ_{eg} .

p	$\langle F \rangle$	$\langle F_{\text{CD}} \rangle$	$\langle F_{2\text{CD}} \rangle$
1	0.27 ± 0.08	0.41 ± 0.17	0.57 ± 0.19
2	0.47 ± 0.16	0.56 ± 0.19	0.73 ± 0.18
3	0.61 ± 0.19	0.68 ± 0.19	0.86 ± 0.14
4	0.70 ± 0.19	0.76 ± 0.19	0.94 ± 0.10
5	0.77 ± 0.19	0.83 ± 0.17	0.99 ± 0.04
6	0.82 ± 0.19	0.89 ± 0.14	1.00 ± 0.01
7	0.86 ± 0.17	0.94 ± 0.11	~ 1
8	0.89 ± 0.17	0.97 ± 0.06	~ 1
9	0.91 ± 0.15	0.99 ± 0.03	~ 1
10	0.93 ± 0.14	~ 1	~ 1

TABLE A1. Average fidelities $\langle F \rangle$, $\langle F_{\text{CD}} \rangle$ and $\langle F_{2\text{CD}} \rangle$ for QAOA, QAOA-CD and QAOA-2CD, respectively, together with their respective standard deviations for all the analyzed p steps. For each fixed p , the QAOA-2CD algorithm outperforms both the QAOA-CD and QAOA algorithms. Values denoted as ~ 1 have standard deviations $\leq 10^{-4}$.

V. CONCLUSIONS

To summarize, in this manuscript we have applied digitized counterdiabatic QAOA algorithms to study fully-connected spin models. In particular we have compared the performances of QAOA, QAOA-CD, QAOA-2CD on a fully-connected disordered MaxCut problem with $N = 5$ vertices. We analyzed $n = 600$ random instances quantifying the quality of the algorithm with the residual energy (i. e., distance between the energy of the calculated solution and the exact ground-state energy) and the fidelity (i. e., the overlap between the exact ground state and the calculated state). Consistently with our prior findings [40], we observe that the QAOA-2CD overperforms the other variants, at the price of an increased number of classical parameters to optimize at fixed p . On the other hand, QAOA-CD and QAOA-2CD perform similarly to QAOA for a fixed number of variational parameters (not shown) [40].

We also analyzed the performances of the algorithms in connection with the gap between the ground state manifold and the first excited state, showing that in general, large gap

p	$\langle \varepsilon_{\text{res}} \rangle$	$\langle \varepsilon_{\text{res,CD}} \rangle$	$\langle \varepsilon_{\text{res,2CD}} \rangle$
1	0.21 ± 0.04	0.15 ± 0.03	0.09 ± 0.03
2	0.11 ± 0.03	0.08 ± 0.02	0.05 ± 0.02
3	0.05 ± 0.02	0.05 ± 0.02	0.026 ± 0.009
4	0.03 ± 0.02	0.03 ± 0.02	0.008 ± 0.003
5	0.02 ± 0.01	0.02 ± 0.01	~ 0
6	0.01 ± 0.01	0.014 ± 0.006	~ 0
7	0.008 ± 0.008	0.006 ± 0.004	~ 0
8	0.006 ± 0.006	0.002 ± 0.001	~ 0
9	0.004 ± 0.004	~ 0	~ 0
10	0.02 ± 0.04	~ 0	~ 0

TABLE A2. Average residual energies $\langle \varepsilon_{\text{res}} \rangle$, $\langle \varepsilon_{\text{res,CD}} \rangle$ and $\langle \varepsilon_{\text{res,2CD}} \rangle$ for QAOA, QAOA-CD and QAOA-2CD, respectively, together with their respective standard deviations for all the analyzed p steps. For each fixed p , the QAOA-2CD algorithm outperforms both the QAOA-CD and QAOA algorithms. Value denoted as ~ 0 have standard deviations $\leq 10^{-4}$.

instances are easier to be solved with this approach. While the role of spectral gaps are well known in QA, in QAOA their role is more subtle and this result is somehow nontrivial. The underlying idea, however, is that a dense spectrum in the vicinity of the ground state makes either the system more prone to be “captured” by local minima during the hybrid optimization procedure or, more likely, the overlap of the variational ground state with the excited states of H_T not negligible. This approach could be used as a starting point to train a neural network with datasets sorted by spectral gaps to approximate efficiently the QAOA angles as done in Ref. [68] for QA.

ACKNOWLEDGMENTS

G. P. and P. L. acknowledge financial support from PNRR MUR Project PE0000023-NQSTI. G. P. acknowledges computational resources from the CINECA award under the ISCR initiative. M. V. and G. P. acknowledge computational resources from MUR, PON “Ricerca e Innovazione 2014-2020”, under Grant No. PIR01_00011 - (I.Bi.S.Co.). This work was supported by PNRR MUR project PE0000023 - NQSTI, by the European Union’s Horizon 2020 research and innovation programme under Grant Agreement No 101017733, by the MUR project CN_00000013-ICSC (P.L.), and by the QuantERA II Programme STAQS project that has received funding from the European Union’s Horizon 2020 research and innovation program.

Appendix A: Numerical results

The numerical results used for Fig. 5 are reported in Tables A1 and A2. Instead, in Tables A3 and A4 we report the zone-resolved fidelities and residual energies, respectively.

In order to provide a more quantitative analysis, Tab. A5 compares the number of steps required to achieve an average fidelity of approximately 1, with a tolerance of 10^{-2} for each algorithm and zone. We see that in **III**-zone (where Δ_{eg} is larger), for all three algorithms, we need fewer steps to reach this tolerance. The lowest value in the table is for QAOA-2CD.

Figs 8 illustrate the fidelity $F_i^{(p)}$ for $n = 600$ random instances of the QAOA for steps $p = 1, 2$ and 7, respectively, for a fully-connected system with $N = 7$ and $N = 9$ spins. In both systems, we split the sorted gaps into three sets of equal cardinalities (200 instances per set). For $N = 7$, the three regions are $\Delta_{eg} \in [0, 0.35]$ (**I**), $\Delta_{eg} \in [0.35, 0.90]$ (**II**), and $\Delta_{eg} \in [0.90, 3.93]$ (**III**). For $N = 9$ spins, the three regions are $\Delta_{eg} \in [0, 0.29]$ (**I**), $\Delta_{eg} \in [0.29, 0.94]$ (**II**), and $\Delta_{eg} \in [0.94, 4.30]$ (**III**). For both systems, we observe a trend consistent with that found for $N = 5$: as the energy gap increases, the algorithm’s performance correspondingly improves. It is evident that as the number of spins in the system increases, the algorithm encounters some challenges in converging to the true ground state. This trend is particularly pronounced for step sizes $p = 1$ and $p = 2$, where the system tends to exhibit smaller average values compared to the case with $N = 5$ spins. Furthermore, the variances observed

p	I-zone			II-zone			III-zone		
	QAOA	QAOA-CD	QAOA-2CD	QAOA	QAOA-CD	QAOA-2CD	QAOA	QAOA-CD	QAOA-2CD
1	0.22 ± 0.05	0.29 ± 0.10	0.40 ± 0.15	0.26 ± 0.05	0.40 ± 0.15	0.57 ± 0.14	0.35 ± 0.08	0.56 ± 0.16	0.74 ± 0.11
2	0.34 ± 0.09	0.40 ± 0.12	0.56 ± 0.19	0.44 ± 0.10	0.55 ± 0.13	0.75 ± 0.10	0.63 ± 0.14	0.75 ± 0.12	0.86 ± 0.07
6	0.60 ± 0.14	0.77 ± 0.19	0.99 ± 0.01	0.87 ± 0.10	0.93 ± 0.04	~ 1	0.98 ± 0.02	0.97 ± 0.02	~ 1
10	0.80 ± 0.18	0.99 ± 0.01	~ 1	0.99 ± 0.02	~ 1	~ 1	0.999 ± 0.002	~ 1	~ 1

TABLE A3. Fidelities for $p = 1, 2, 6, 10$, in the three zones identified in the main text by the range of the minimum gap Δ_{eg} . We compare QAOA, QAOA-CD and QAOA-2CD. Values denoted as ~ 1 have standard deviations $\sigma \leq 10^{-4}$.

p	I-zone			II-zone			III-zone		
	QAOA	QAOA-CD	QAOA-2CD	QAOA	QAOA-CD	QAOA-2CD	QAOA	QAOA-CD	QAOA-2CD
1	0.17 ± 0.03	0.14 ± 0.03	0.09 ± 0.03	0.21 ± 0.03	0.16 ± 0.03	0.10 ± 0.03	0.25 ± 0.03	0.18 ± 0.04	0.10 ± 0.04
2	0.08 ± 0.02	0.08 ± 0.02	0.05 ± 0.02	0.11 ± 0.02	0.10 ± 0.02	0.06 ± 0.02	0.12 ± 0.03	0.09 ± 0.03	0.06 ± 0.02
6	0.017 ± 0.008	0.014 ± 0.006	~ 0	0.017 ± 0.009	0.016 ± 0.006	~ 0	0.003 ± 0.004	0.011 ± 0.006	~ 0
10	0.006 ± 0.003	~ 0	~ 0	0.002 ± 0.003	~ 0	~ 0	~ 0	~ 0	~ 0

TABLE A4. Residual energies for $p = 1, 2, 6, 10$, in the three zones identified in the main text by the range of the minimum gap Δ_{eg} . We compare QAOA, QAOA-CD and QAOA-2CD. Values denoted as ~ 0 have standard deviations $\sigma \leq 10^{-4}$.

in these cases are significantly larger than those observed for the $N = 5$ system. These findings suggest that the increased system size introduces additional challenges in accurately determining the ground state, both in terms of mean values and the variability of the results. This behavior highlights the growing complexity of the problem as the number of spins increases.

Appendix B: Minimization

In this section, we examine the classical minimization aspect of our approach in detail. The cost function, as defined in Eq. (7), presents a challenging landscape characterized by high complexity and the presence of numerous local minima. This complexity poses a significant challenge for the minimization process, as the minimizer may easily become trapped within one of these local minima, hindering convergence to a global minimum.

To mitigate this risk and enhance the overall effectiveness of the algorithm, we employ a strategy involving multiple independent minimization attempts. Specifically, at each step, we initiate $S = 20$ separate minimizations of the cost function from Eq. (7), each starting from a random set of initial angles. By adopting this approach, we aim to increase the chances of achieving a result closer to the global minimum, as the multiple initializations help explore different regions of the solution space more effectively.

Moreover, during our analysis, we identified instances with non-monotonic behavior as a function of p . Upon increasing the value of S , we observed a shift toward a monotonic behavior in the resulting curves. This observation suggests that a larger number of initializations with distinct starting angles can improve the stability of the minimization process and contribute to more consistent convergence patterns.

Fig. 9 shows the cost function of QAOA at step $p = 1$ in Eq. (7) for a spin system of size $N = 5$, for three specific instances. Panel (a) illustrates the instance with the smallest energy gap, Δ_{eg} , among those studied, with $\Delta_{eg} = 0.002$. Panel (b) shows the cost function for an instance characterized by $\Delta_{eg} = 1.98$. Lastly, panel (c) displays the cost function for the instance with the largest observed gap, where $\Delta_{eg} = 4.745$.

For each of these cost functions, the figure includes the minimization path in red, illustrating the trajectory followed during minimization for a specific set of initial angles. Notably, we selected the initial angles that, as determined through poste-

	QAOA	QAOA-CD	QAOA-2CD
I -zone	$p > 10$	$p = 10$	$p = 6$
II -zone	$p = 10$	$p = 6$	$p = 4$
III -zone	$p = 6$	$p = 6$	$p = 2$

TABLE A5. The number of steps required to achieve an average fidelity of approximately 1 with a tolerance of 10^{-2} . The values are then compared with respect to the different algorithms and different zones, depending on the value of Δ_{eg} . The lowest value is observed for QAOA-2CD in the **III**-zone.

rior analysis, led to the best minimum (white star) achieved for each case.

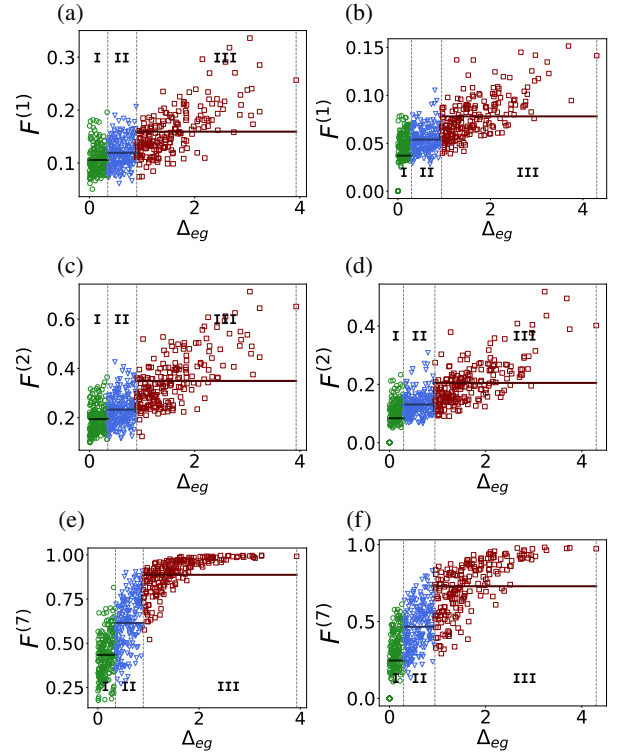


FIG. 8. Fidelity $F_i^{(p)}$ as a function of the minimal gap Δ_{eg} for QAOA. Panels (a, c, e) are for $N = 7$ spins, while panels (b, d, f) are for $N = 9$. The different rows correspond to $p = 1$, $p = 2$, $p = 7$, respectively. Three distinct regions based on the energy gap separating the ground state from the first excited state can be singled as described in the main text. The horizontal line within each sector depicts the corresponding average value of that sector.

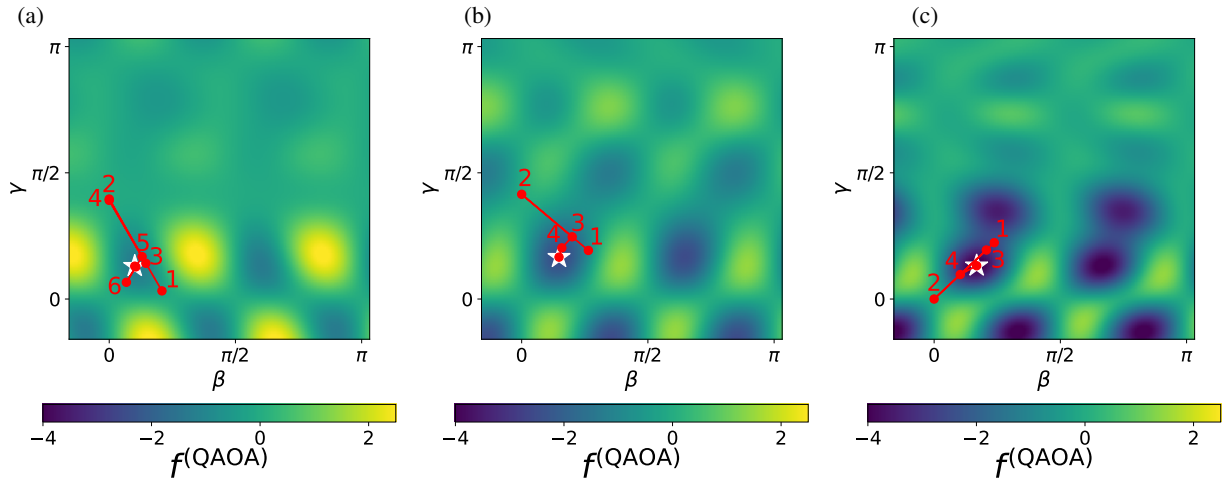


FIG. 9. QAOA cost function (see Eq. (7)) at step $p = 1$ for spin $N = 5$ for three different instances. Panel a) shows cost function of the instance with lowest Δ_{eg} ($\Delta_{eg} = 0.002$) among all random instances analyzed, panel b) an instance with $\Delta_{eg} = 1.98$ and in panel c) cost function of the instance with the largest Δ_{eg} among the instances analyzed $\Delta_{eg} = 4.745$. The red segments illustrate the minimization path taken from a selected set of random initial angles. These particular angles were chosen based on a posterior analysis, as they led to the best minimum found in each case, marked by a white star in the figures.

- [1] M. Cerezo, A. Arrasmith, R. Babbush, S. C. Benjamin, S. Endo, K. Fujii, J. R. McClean, K. Mitarai, X. Yuan, L. Cincio, *et al.*, *Nature Reviews Physics* **3**, 625 (2021).
- [2] J. I. Colless, V. V. Ramasesh, D. Dahlen, M. S. Blok, M. E. Kimchi-Schwartz, J. R. McClean, J. Carter, W. A. de Jong, and I. Siddiqi, *Phys. Rev. X* **8**, 011021 (2018).
- [3] H. R. Grimsley, S. E. Economou, E. Barnes, and N. J. Mayhall, *Nature communications* **10**, 3007 (2019).
- [4] A. Kandala, A. Mezzacapo, K. Temme, M. Takita, M. Brink, J. M. Chow, and J. M. Gambetta, *nature* **549**, 242 (2017).
- [5] J. Yao, L. Lin, and M. Bukov, *Phys. Rev. X* **11**, 031070 (2021).
- [6] H. Zhang, X. Xu, C. Zhang, M.-H. Yung, T. Huang, and Y. Liu, *Phys. Rev. A* **108**, 042611 (2023).
- [7] E. Anschuetz, J. Olson, A. Aspuru-Guzik, and Y. Cao, in *Quantum Technology and Optimization Problems*, edited by S. Feld and C. Linnhoff-Popien (Springer International Publishing, Cham, 2019) pp. 74–85.
- [8] A. H. Karamlou, W. A. Simon, A. Katabarwa, T. L. Scholten, B. Peropadre, and Y. Cao, *npj Quantum Information* **7**, 156 (2021).
- [9] E. Farhi, J. Goldstone, and S. Gutmann, A quantum approximate optimization algorithm (2014), [arXiv:1411.4028 \[quant-ph\]](https://arxiv.org/abs/1411.4028).
- [10] S. M. Venkatesh, A. Macaluso, M. Nuske, M. Klusch, and A. Dengel, Qubit-efficient variational quantum algorithms for image segmentation (2024), [arXiv:2405.14405 \[cs.CV\]](https://arxiv.org/abs/2405.14405).
- [11] B. G. Sarmina, G.-H. Sun, and S.-H. Dong, Parameter optimization comparison in qaoa using stochastic hill climbing with random re-starts and local search with entangled and non-entangled mixing operators (2024), [arXiv:2405.08941 \[quant-ph\]](https://arxiv.org/abs/2405.08941).
- [12] J. A. Montanez-Barrera and K. Michielsen, Towards a universal qaoa protocol: Evidence of quantum advantage in solving combinatorial optimization problems (2024), [arXiv:2405.09169 \[quant-ph\]](https://arxiv.org/abs/2405.09169).
- [13] B. Tselikhovskiy, I. Safro, and Y. Alexeev, Equivariant qaoa and the duel of the mixers (2024), [arXiv:2405.07211 \[quant-ph\]](https://arxiv.org/abs/2405.07211).
- [14] C. Boy and D. J. Wales, *Phys. Rev. A* **109**, 062602 (2024).
- [15] A. Lucas, *Frontiers in Physics* **2**, 10.3389/fphy.2014.00005 (2014).
- [16] S. Hadfield, Z. Wang, B. O’Gorman, E. G. Rieffel, D. Venturelli, and R. Biswas, *Algorithms* **12**, 10.3390/a12020034 (2019).
- [17] A. Bärttschi and S. Eidenbenz, in *2020 IEEE International Conference on Quantum Computing and Engineering (QCE)* (2020) pp. 72–82.
- [18] J. Villalba-Diez, A. González-Marcos, and J. B. Ordieres-Meré, *Sensors* **22**, 10.3390/s22010244 (2022).
- [19] J. Golden, A. Bärttschi, D. O’Malley, and S. Eidenbenz, in *2021 IEEE International Conference on Quantum Computing and Engineering (QCE)* (2021) pp. 137–147.
- [20] F. G. Fuchs, K. O. Lye, H. Møll Nilsen, A. J. Stasik, and G. Sartor, *Algorithms* **15**, 10.3390/a15060202 (2022).
- [21] D. J. Egger, J. Mareček, and S. Woerner, *Quantum* **5**, 479 (2021).
- [22] T. Yoshioka, K. Sasada, Y. Nakano, and K. Fujii, *Phys. Rev. Res.* **5**, 023071 (2023).
- [23] J. Wurtz and P. J. Love, *IEEE Transactions on Quantum Engineering* **2**, 1 (2021).
- [24] A. Gomez Cadavid, I. Montalban, A. Dalal, E. Solano, and N. N. Hegade, *arXiv e-prints* (2023), [2308.15475 \[quant-ph\]](https://arxiv.org/abs/2308.15475).
- [25] Y. Ji, K. F. Koenig, and I. Polian, Improving the performance of digitized counterdiabatic quantum optimization via algorithm-oriented qubit mapping (2023), [arXiv:2311.14624 \[quant-ph\]](https://arxiv.org/abs/2311.14624).
- [26] Y. Yu, C. Cao, C. Dewey, X.-B. Wang, N. Shannon, and R. Joynt, *Phys. Rev. Res.* **4**, 023249 (2022).
- [27] L. Zhu, H. L. Tang, G. S. Barron, F. A. Calderon-Vargas, N. J. Mayhall, E. Barnes, and S. E. Economou, *Phys. Rev. Res.* **4**, 033029 (2022).
- [28] S. Bravyi, A. Kliesch, R. Koenig, and E. Tang, *Phys. Rev. Lett.* **125**, 260505 (2020).
- [29] P. Zou, Multiscale quantum approximate optimization algorithm (2023), [arXiv:2312.06181 \[quant-ph\]](https://arxiv.org/abs/2312.06181).
- [30] A. B. Magann, K. M. Rudinger, M. D. Grace, and M. Sarovar, *Phys. Rev. Lett.* **129**, 250502 (2022).
- [31] K. Blekos, D. Brand, A. Ceschini, C.-H. Chou, R.-H. Li, K. Pandya, and A. Summer, *Physics Reports* **1068**, 1 (2024).
- [32] A. Misra-Spieldenner, T. Bode, P. K. Schuhmacher, T. Stollenwerk, D. Bagrets, and F. K. Wilhelm, *PRX Quantum* **4**, 030335 (2023).
- [33] P. Chandarana, N. N. Hegade, K. Paul, F. Albarrán-Arriagada, E. Solano, A. del Campo, and X. Chen, *Phys. Rev. Research* **4**, 013141 (2022).
- [34] Y. Chai, Y.-J. Han, Y.-C. Wu, Y. Li, M. Dou, and G.-P. Guo, *Phys. Rev. A* **105**, 042415 (2022).
- [35] J. Wurtz and P. J. Love, *Quantum* **6**, 635 (2022).
- [36] P. Chandarana, N. N. Hegade, I. Montalban, E. Solano, and X. Chen, *Phys. Rev. Appl.* **20**, 014024 (2023).
- [37] M. Chalupnik, H. Melo, Y. Alexeev, and A. Galda, in *2022 IEEE International Conference on Quantum Computing and Engineering (QCE)* (2022) pp. 97–103.
- [38] X. Chen, I. Lizuain, A. Ruschhaupt, D. Guéry-Odelin, and J. G. Muga, *Phys. Rev. Lett.* **105**, 123003 (2010).
- [39] D. Guéry-Odelin, A. Ruschhaupt, A. Kiely, E. Torrontegui, S. Martínez-Garaot, and J. G. Muga, *Rev. Mod. Phys.* **91**, 045001 (2019).
- [40] M. Vizzuso, G. Passarelli, G. Cantele, and P. Lucignano, *New Journal of Physics* (2023).
- [41] T. Albash and D. A. Lidar, *Rev. Mod. Phys.* **90**, 015002 (2018).
- [42] N. White, K. Gui, Z. Saleem, and M. Suchara, in *APS March Meeting Abstracts*, APS Meeting Abstracts, Vol. 2021 (2021) p. H71.157.
- [43] K. L. Hoffman and M. Padberg, Traveling salesman problem (tsp)traveling salesman problem, in *Encyclopedia of Operations Research and Management Science*, edited by S. I. Gass and C. M. Harris (Springer US, New York, NY, 2001) pp. 849–853.
- [44] R. Graham and P. Hell, *Annals of the History of Computing* **7**, 43 (1985).
- [45] H. M. Salkin and C. A. De Kluyver, *Naval Research Logistics Quarterly* **22**, 127–144 (1975).
- [46] C. H. Papadimitriou and K. Steiglitz, *Combinatorial optimization: algorithms and complexity* (Courier Corporation, 1998).
- [47] L. Trevisan, *SIAM Journal on Computing* **41**, 1769 (2012), <https://doi.org/10.1137/090773714>.
- [48] F. Barahona, *Operations Research Letters* **2**, 107 (1983).
- [49] S. Poljak and F. Rendl, *Discrete Applied Mathematics* **62**, 249 (1995).
- [50] S. Cook, *Clay Mathematics Institute* **2**, 6 (2000).
- [51] T. Kadowaki and H. Nishimori, *Phys. Rev. E* **58**, 5355 (1998).
- [52] P. Serafini, in *Multiple Criteria Decision Making*, edited by G. H. Tzeng, H. F. Wang, U. P. Wen, and P. L. Yu (Springer New York, New York, NY, 1994) pp. 283–292.
- [53] P. R. Hegde, G. Passarelli, A. Scocco, and P. Lucignano, *Phys. Rev. A* **105**, 012612 (2022).
- [54] G. Passarelli, V. Cataudella, and P. Lucignano, *Phys. Rev. B* **100**,

- 024302 (2019).
- [55] G. Passarelli, K.-W. Yip, D. A. Lidar, H. Nishimori, and P. Lucignano, *Phys. Rev. A* **101**, 022331 (2020).
 - [56] G. Passarelli, V. Cataudella, R. Fazio, and P. Lucignano, *Phys. Rev. Research* **2**, 013283 (2020).
 - [57] G. Passarelli, G. De Filippis, V. Cataudella, and P. Lucignano, *Phys. Rev. A* **97**, 022319 (2018).
 - [58] G. Passarelli, R. Fazio, and P. Lucignano, *Phys. Rev. A* **105**, 022618 (2022).
 - [59] G. Passarelli, K.-W. Yip, D. A. Lidar, and P. Lucignano, *Phys. Rev. A* **105**, 032431 (2022).
 - [60] G. Passarelli and P. Lucignano, *Phys. Rev. A* **107**, 022607 (2023).
 - [61] P. R. Hegde, G. Passarelli, G. Cantele, and P. Lucignano, *New Journal of Physics* [10.1088/1367-2630/ace547](https://doi.org/10.1088/1367-2630/ace547) (2023).
 - [62] E. Farhi, J. Goldstone, S. Gutmann, and M. Sipser, arXiv e-prints (2000), [arXiv:quant-ph/0001106](https://arxiv.org/abs/quant-ph/0001106) [quant-ph].
 - [63] A. del Campo, *Phys. Rev. Lett.* **111**, 100502 (2013).
 - [64] F. Casas, A. Murua, and M. Nadinic, *Computer Physics Communications* **183**, 2386 (2012).
 - [65] R. H. Byrd, P. Lu, J. Nocedal, and C. Zhu, *SIAM Journal on Scientific Computing* **16**, 1190 (1995), <https://doi.org/10.1137/0916069>.
 - [66] G. E. Santoro, R. Martoňák, E. Tosatti, and R. Car, *Science* **295**, 2427 (2002).
 - [67] L. Zhou, S.-T. Wang, S. Choi, H. Pichler, and M. D. Lukin, *Phys. Rev. X* **10**, 021067 (2020).
 - [68] G. Bishop, S. Montangero, and F. K. Wilhelm, A set of annealing protocols for optimized system dynamics and classification of fully connected spin glass problems (2023), [arXiv:2310.10442](https://arxiv.org/abs/2310.10442) [quant-ph].
 - [69] T. Kato, *Journal of the Physical Society of Japan* **5**, 435 (1950), <https://doi.org/10.1143/JPSJ.5.435>.